



# Multilevel hybrid accurate handcrafted model for myocardial infarction classification using ECG signals

Prabal Datta Barua<sup>1,2</sup> · Emrah Aydemir<sup>3</sup> · Sengul Dogan<sup>4</sup>  · Mehmet Ali Kobat<sup>5</sup> · Fahrettin Burak Demir<sup>6</sup> · Mehmet Baygin<sup>7</sup> · Turker Tuncer<sup>4</sup> · Shu Lih Oh<sup>8</sup> · Ru-San Tan<sup>9,10</sup> · U. Rajendra Acharya<sup>8,11,12</sup>

Received: 30 March 2022 / Accepted: 3 November 2022 / Published online: 28 November 2022  
© The Author(s), under exclusive licence to Springer-Verlag GmbH Germany, part of Springer Nature 2022

## Abstract

Myocardial infarction (MI) is detected using electrocardiography (ECG) signals. Machine learning (ML) models have been used for automated MI detection on ECG signals. Deep learning models generally yield high classification performance but are computationally intensive. We have developed a novel multilevel hybrid feature extraction-based classification model with low time complexity for MI classification. The study dataset comprising 12-lead ECGs belonging to one healthy and 10 MI classes were downloaded from a public ECG signal databank. The model architecture comprised multilevel hybrid feature extraction, iterative feature selection, classification, and iterative majority voting (IMV). In the hybrid handcrafted feature (HHF) generation phase, both textural and statistical feature extraction functions were used to extract features from ECG beats but only at a low level. A new pooling-based multilevel decomposition model was presented to enable them to create features at a high level. This model used average and maximum pooling to create decomposed signals. Using these pooling functions, an unbalanced tree was obtained. Therefore, this model was named multilevel unbalanced pooling tree transformation (MUPTT). On the feature extraction side, two extractors (functions) were used to generate both statistical and textural features. To generate statistical features, 20 commonly used moments were used. A new, improved symmetric binary pattern function was proposed to generate textural features. Both feature extractors were applied to the original MI signal and the decomposed signals generated by the MUPTT. The most valuable features from among the extracted feature vectors were selected using iterative neighborhood component analysis (INCA). In the classification phase, a one-dimensional nearest neighbor classifier with ten-fold cross-validation was used to obtain lead-wise results. The computed lead-wise results derived from all 12 leads of the same beat were input to the IMV algorithm to generate ten voted results. The most representative was chosen using a greedy technique to calculate the overall classification performance of the model. The HHF-MUPTT-based ECG beat classification model attained excellent performance, with the best lead-wise accuracy of 99.85% observed in Lead III and 99.94% classification accuracy using the IMV algorithm. The results confirmed the high MI classification ability of the presented computationally lightweight HHF-MUPTT-based model.

**Keywords** Local binary pattern · Statistical feature extraction · MI classification · ECG signal processing

## 1 Introduction

Myocardial infarction (MI) occurs when the sudden cessation of blood flow in a coronary artery due to occlusion, which results in the death of the part of the heart muscle supplied by the artery. The occlusion is almost always caused by acute thrombosis of the culprit infarct artery [1] induced by inflammation [2] and release of thrombogenic factors

[3] at a location overlying a ruptured atherosclerotic plaque [4] that has formed from the progressive accumulation of cholesterol, fat, and fibrin in the coronary artery wall [5]. Depending on the coronary artery involved, different areas of the heart undergo cell death that disrupts local regional myocardial contractility and electrical activation/conduction [6] in the affected muscle. Surface electrocardiography (ECG), which is routinely used in the acute emergency setting to diagnose MI in patients presenting with characteristic chest pain symptoms [7], maps out the underlying areas of MI-induced perturbed electrical activation, thus offering a window to the location and extent of heart muscle damage,

✉ Sengul Dogan  
sdogan@firat.edu.tr; turkertuncer@firat.edu.tr

Extended author information available on the last page of the article

which is of prognostic significance. Additionally, MI localization provides advanced information on the putative culprit coronary artery, which is useful for planning the approach during acute percutaneous coronary intervention for revascularization [8].

Manual interpretation of the ECG requires experts, which may not always be accessible, especially in smaller district medical facilities or in emergency ambulances in transit. Many different decision support systems based on machine learning (ML) have been developed to assist doctors and paramedical personnel in diagnosing MI [9–11]. These studies have reported high accuracy rates with machine learning techniques [12–14]. Rahman et al. [15] proposed an ECG-based model for detecting five classes (Covid-19, MI, abnormal heartbeat, recovered MI, and normal), which they trained. They tested on a dataset comprising 250 Covid-19, 77 MI, 548 abnormal heartbeats, 203 recovered MI, and 859 normal ECG images. After data augmentation to balance classes in the dataset, they obtained 97.83% classification accuracy with InceptionV3 for the five classes. Jahmunah et al. [16] proposed a model based on Gabor convolutional neural networks for four-class classification of normal, MI, coronary artery disease, and congestive heart failure using ECG signals. Their study dataset comprised 84,703 normal, 20,265 MI, 15,300 coronary artery disease, and 30,000 congestive heart failure ECG segments. They achieved accuracy rates of 99.55% and 98.74% for convolutional neural networks and Gabor convolutional neural networks, respectively. Gibson et al. [17] proposed a one-dimensional convolutional neural network for the detection of MI using single-lead ECG signals. They attained 90.50% accuracy for binary classification of ST-elevation versus non-ST-elevation MI. Sharma et al. [18] used an optimal biorthogonal filter bank to develop a model for MI diagnosis. On their study dataset of ECGs from 148 MI and 52 normal subjects, their model attained 99.74% binary classification accuracy. Darmawahyuni et al. [19] applied long short-term memory and recurrent neural network to their model for MI classification. In their database of ECG signals of 290 subjects, they attained balanced accuracy of 83.00%.

### 1.1 Motivation and our model

ECG signal classification is an important area of research at the intersection of ML and cardiology. Many works/studies have been published on using ECG-based ML models to diagnose diverse cardiological conditions. While known to yield high performance, deep learning models are constrained by high computational demands. In contrast, hand-crafted models have lower time complexities but usually cannot attain high performance since the features are generated at a low level. To overcome this problem, a hybrid hand-crafted feature (HHF) engineering method was proposed

that could extract features at multiple levels. In our model, textural and statistical feature extraction using one-dimensional improved symmetric binary pattern (1D-ISBP) and 20 common statistical moments were combined with multilevel unbalanced pooling tree transformation (MUPTT), which enabled the extraction of features at both high and low levels. The most valuable features were selected using iterative neighborhood component analysis (INCA). The selected features were classified using a shallow k-nearest neighbor (kNN)-based classifier, one-dimensional nearest neighbor (1NN), with tenfold cross-validation (CV) to yield lead-wise results. Finally, lead-wise results from all 12 leads corresponding to a single beat were input to an iterative majority voting (IMV) algorithm to choose the most representative lead for classification using 1NN. The proposed model attained excellent accuracy for MI classification using both lead-wise and IMV outputs.

### 1.2 Novelties and contributions

We proposed two novel functions, and these functions are 1D-ISBP and MUPTT. To extract distinctive textural features from an ECG signal, we proposed 1D-ISBP. In the advanced signal classification models, transformations have been used to extract features in the frequency domain to get high classification ability. Moreover, deep learning models (especially CNNs) have been used as pooling functions. We mimicked deep learning networks to propose this classification model. However, pooling functions have a routing problem. For instance, maximum pooling routes only peak values and average pooling routes only average values. To handle this problem, we proposed MUPTT. MUPTT is a multiple pooling-based multilevel transformations. This research proposes an accurate ECG signal classification model by deploying these methods (MUPTT, 1D-ISBP, statistical feature generation, iterative feature selector, classifier, and IMV).

Novelties and contributions of the presented HHF-MUPTT-based MI classification model are listed below.

Novelties:

- Pooling functions have commonly been used in deep learning networks. In this work, we presented a hand-crafted features-based model in which we mimicked deep networks to attain high classification results using simple models. A new pooling pooling-based transformation named MUPTT was proposed to create a multilevel feature generator.
- A new, improved textural feature extractor, 1D-ISBP, was presented as an improved version of the center symmetric local binary pattern (CSLBP) [20].

Contributions:

- In this work, we used handcrafted models to propose an effective one-dimensional signal classification architecture. A good feature engineering model must extract multilevel features and eliminate redundant features to attain high classification ability. The other advantage of the handcrafted features-based models is low running time. However, the handcrafted feature extractors cannot extract features at high level. Handcrafted features can be divided into two main types: textural and statistical. In our model, we assembled 1D-ISBP and statistical feature extraction functions with MUPTT to extract features with low time complexity at high and low levels.
- The model was tested on a 200-subject (148 MI and 52 healthy) 12-lead ECG dataset with 49,235 analyzable ECG beats of 11 classes (10 MI and one healthy). Our model attained excellent MI accuracy rates (97.93% to 99.85%) on lead-wise classification using a shallow 1NN classifier with a tenfold CV. Moreover, IMV was used to select the best ECG lead, which improved the model classification accuracy to 99.94%.

## 2 Dataset

We used an ECG heartbeat database downloaded from the Physiobank database [21]. This dataset comprises 12-lead ECGs of 200 subjects (52 normal and 148 MI patients) divided into 10 MI classes and one healthy class. Table 1 shows the attributes of the study dataset by class and lead position. Example ECG beats of all classes are shown in Fig. 1.

As the ECG signals had been sampled at different rates, they were all re-sampled at 1000 Hz. Signal noise and baseline shift were eliminated by applying wavelet transform. In addition, R peak detection was performed using the

Pan-Tompkin’s algorithm [22]. Individual beats were segmented by selecting 250 and 400 samples to the left and right of the R peak, respectively, to ensure adequate coverage of the QRS complex and the following ST-segment for each beat (total of 651 samples per beat). The total number of beats for every lead is identical (see last row in Table 1). As the model used IMV to select the best representative leads for classification, which required an identical number of beats in every lead, the lowest common denominator of 49,235 individual beats where R peaks had been detected successfully in all 12 ECG leads (and were present in all 12 leads at the same time) were selected for analysis (Table 2).

## 3 The proposed hand-modeled ECG signal classification model

The proposed feature engineering model comprises four primary phases: multilevel hybrid handcrafted feature generation; feature selection using INCA; classification using kNN with ten-fold CV; and IMV (Fig. 2). In the first phase, handcrafted features of the ECG beats were generated using 1D-ISBP, a statistical feature generator, and MUPTT. A six-leveled MUPTT was used, where the number of levels was determined by the length of the ECG beat (651) and the size of the overlapping block used for feature extraction in 1D-ISBP (9) as given by the formula  $\lceil \log_2 \left( \frac{651}{9} \right) \rceil = 6$ . In the six-leveled MUPTT, six average pooling bands and six maximum pooling bands were generated. Both feature generators (1D-ISBP and statistical feature generator) extracted features from each input ECG beat and the wavelet subbands generated by the MUPTT. Hence, 13 feature vectors (1, 6, and 6 vectors generated from the ECG beat, average pooling

**Table 1** Attributes of the used ECG beat dataset

| Class | Leads  |        |        |        |        |        |        |        |        |        |        |        | Total   |
|-------|--------|--------|--------|--------|--------|--------|--------|--------|--------|--------|--------|--------|---------|
|       | I      | II     | III    | aVR    | aVL    | aVF    | V1     | V2     | V3     | V4     | V5     | V6     |         |
| H     | 10,598 | 10,546 | 10,574 | 10,494 | 10,537 | 10,472 | 10,482 | 10,483 | 10,450 | 10,371 | 10,322 | 10,323 | 125,652 |
| A     | 4902   | 4861   | 4993   | 4720   | 4882   | 4941   | 4742   | 4741   | 4743   | 4745   | 4743   | 4741   | 57,754  |
| AL    | 6424   | 6467   | 6360   | 6579   | 6676   | 6520   | 6501   | 6538   | 6540   | 6397   | 6589   | 6514   | 78,105  |
| AS    | 8146   | 8024   | 8260   | 8153   | 8146   | 8567   | 8152   | 8148   | 8238   | 8429   | 8151   | 8152   | 98,566  |
| I     | 10,592 | 10,691 | 11,522 | 10,588 | 11,161 | 11,008 | 10,502 | 10,671 | 10,711 | 10,591 | 10,589 | 10,589 | 129,215 |
| IL    | 5911   | 5888   | 5919   | 5911   | 5909   | 6047   | 5900   | 5932   | 5914   | 5912   | 5861   | 5882   | 70,986  |
| IP    | 48     | 48     | 48     | 48     | 48     | 48     | 48     | 48     | 48     | 48     | 48     | 48     | 576     |
| IPL   | 2516   | 2512   | 2517   | 2516   | 2518   | 2520   | 2515   | 2503   | 2516   | 2516   | 2516   | 2516   | 30,181  |
| L     | 459    | 459    | 460    | 459    | 470    | 459    | 459    | 459    | 459    | 459    | 459    | 459    | 5520    |
| P     | 460    | 460    | 459    | 460    | 460    | 460    | 460    | 461    | 463    | 460    | 460    | 460    | 5523    |
| PL    | 777    | 772    | 777    | 778    | 779    | 778    | 779    | 778    | 777    | 777    | 777    | 777    | 9326    |
| Total | 50,833 | 50,728 | 51,889 | 50,706 | 51,586 | 51,820 | 50,540 | 50,762 | 50,859 | 50,705 | 50,515 | 50,461 | 611,404 |

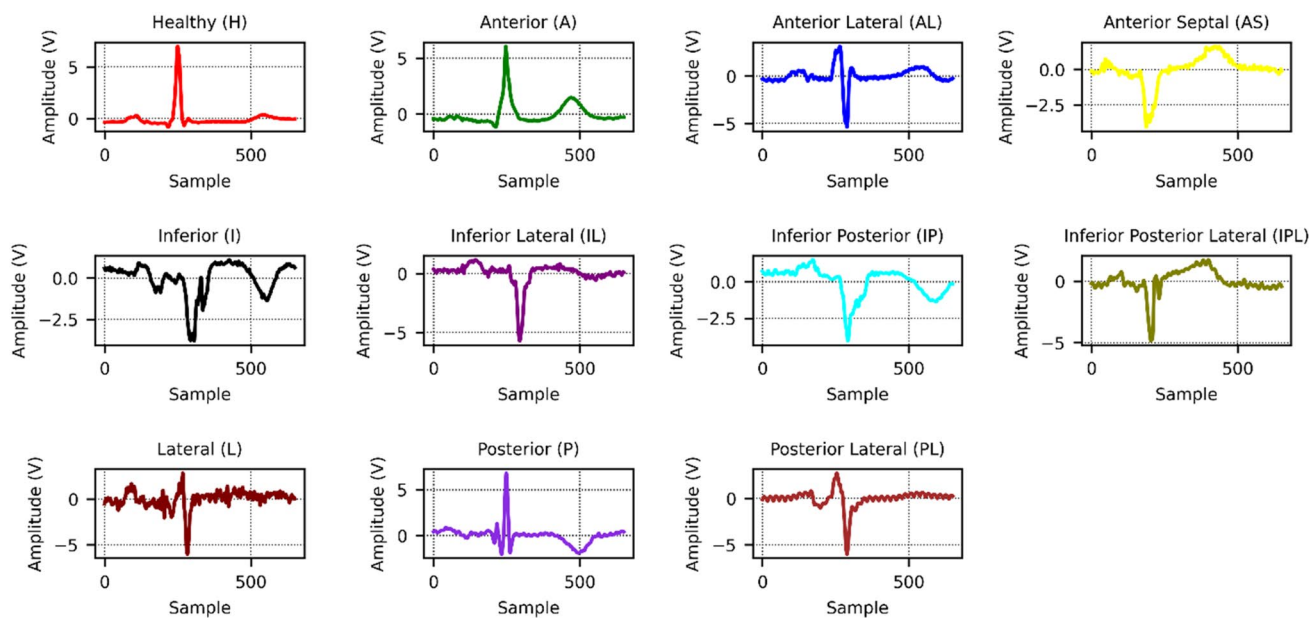


**Fig. 1** Lead III waveforms on example ECG signals of different classes in the dataset

**Table 2** Total number of ECG beats in all leads by myocardial infarct class

| No.   | Class                            | Number of beats |
|-------|----------------------------------|-----------------|
| 0     | Healthy (H)                      | 10,305          |
| 1     | Anterior (A)                     | 4659            |
| 2     | Anterior lateral (AL)            | 6142            |
| 3     | Anterior septal (AS)             | 7976            |
| 4     | Inferior (I)                     | 10,215          |
| 5     | Inferior lateral (IL)            | 5822            |
| 6     | Inferior posterior (IP)          | 48              |
| 7     | Inferior posterior lateral (IPL) | 2495            |
| 8     | Lateral (L)                      | 459             |
| 9     | Posterior (P)                    | 459             |
| 10    | Posterior lateral (PL)           | 655             |
| Total |                                  | 49,235          |

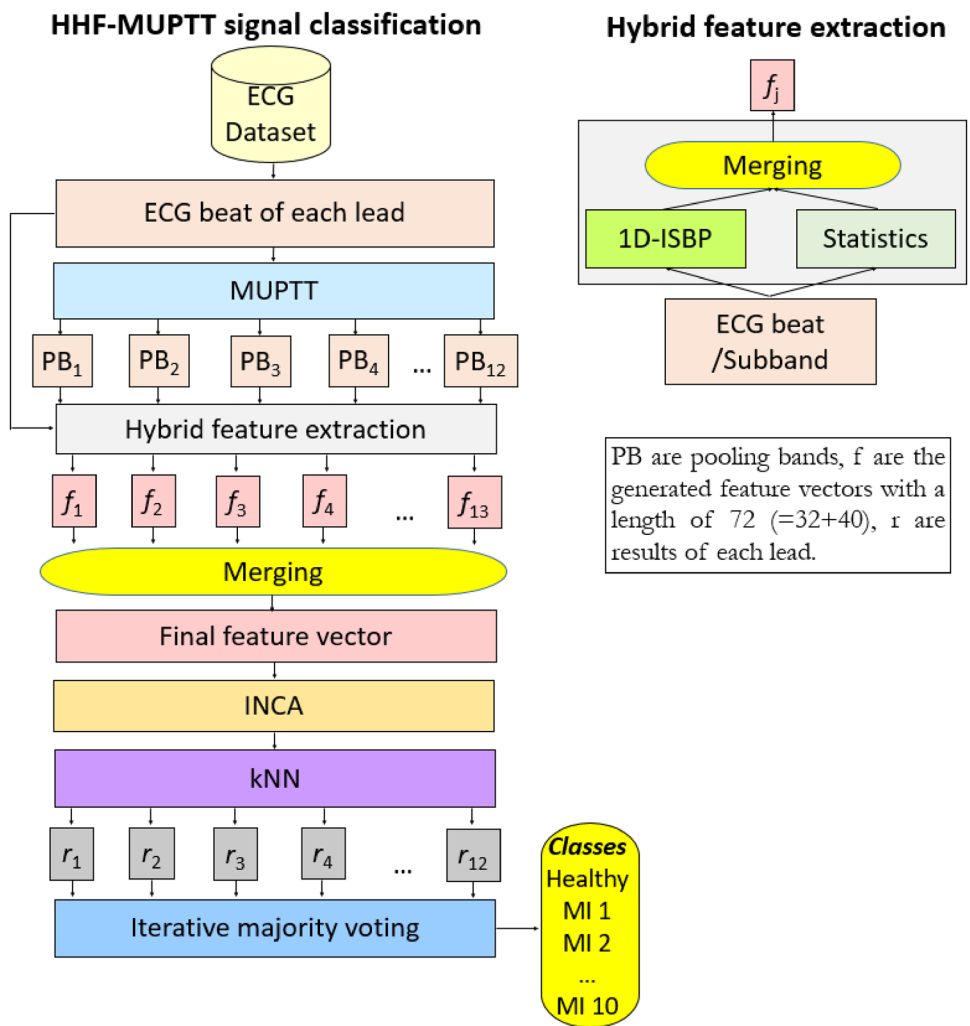
bands, and maximum pooling bands, respectively) were generated, each with a length equal to 72 (32 and 40 features generated by 1D-ISBP and statistical feature generator, respectively) for each input ECG beat. These feature vectors were concatenated to form a final feature vector of length 936 ( $= 72 \times 13$ ). INCA, an iterative version of the distance-based feature selector neighborhood component analysis (NCA), was employed to choose the top features from the

final feature vector generated in the feature extraction phase. In this role, NCA can be viewed as the selection version of kNN. To improve NCA's feature selection ability, INCA uses two additional parameters: loop range and misclassification/loss rate calculator. The best features selected by INCA were then fed to the kNN classifier for classification using a ten-fold CV, which yielded one lead-wise result. The results of all 12 leads corresponding to the same single beat on the source 12-lead ECG were collated. IMV algorithm was applied to generate 10 voted results, from which the best one was chosen to represent the general majority voting result.

The ECG signal of each lead is read, and wavelet subbands are generated by deploying a MUPTT. Using MUPTT (average and maximum pooling functions with six levels), 12 pooled bands (PB) are generated. The presented hybrid feature extractor (1D-ISBP + statistical feature generator) generates feature vectors ( $f$ ) from each of the 12 subbands and the raw input ECG beat. The 13 feature vectors generated are merged to obtain the final feature vector. INCA chooses/selects the top valuable/useful features, which are then classified using the kNN classifier for lead-wise results ( $r$ ). Finally, by deploying IMV, the voted results are calculated.

Our proposed ECG signal classification architecture is illustrated in Fig. 2. More details and steps of the

**Fig. 2** Schema of the proposed HHF-MUPTT-based ECG beats classification model



architecture of the HHF-MUPTT-based ECG classification are explained in the sections on the model’s feature extraction, feature selection, and classification phases below.

**3.1 Feature extraction**

**Step 0:** Read/load each ECG beats of each channel.

**Step 1:** Apply six-leveled  $\left\lceil \left(6 = \log_2 \left(\frac{651}{9}\right)\right) \right\rceil$  MUPTT to the ECG beat. In this decomposition, average pooling and maximum pooling are used to create child nodes of the created unbalanced tree. Using a single pooling function, a routing problem will occur. By using two pooling functions, this problem is resolved with decomposition. The mathematical operations of the MUPTT are given below.

$$A_1 = AP(ECG), \tag{1}$$

$$M_1 = MP(ECG), \tag{2}$$

$$A_h = AP(A_{h-1}), h \in \{2, 3, \dots, 6\}, \tag{3}$$

$$M_h = MP(A_{h-1}), \tag{4}$$

where  $M$  and  $A$  are the decomposed signals/bands maximum, and average pooling, respectively;  $MP(\cdot)$  is the maximum pooling function,  $AP(\cdot)$  defines the average pooling function; and  $ECG$  represents the input ECG beat signal. Maximum and average pooling functions use non-overlapping windows with a length of two. To better explain the used pooling function, pseudocodes of these functions are given below (see Algorithm 1 and Algorithm 2).

Algorithm 1. Pseudocode of the used average pooling.

|   |
|---|
| <b>Function:</b> $AP(sig)$  |
| <b>Input:</b> One-dimensional signal ( $sig$ ) with a length of $L$ .   |
| <b>Output:</b> The created pooled signal ( $A$ ) with a length of $\lfloor \frac{L}{2} \rfloor$ .   |
| <pre> 00: Load one-dimensional signal. 01: c=1; // Counter defining. 02: for j=1 to L step by 2 do 03:   for t=1 to 2 do 04:     block(t) = sig(t + j - 1); // Non-overlapping block creation. 05:   end for t 06:   A(c) = <math>\frac{1}{2} \sum_{j=1}^2 block(j)</math>; 07:   c = c + 1; 08: end for j </pre> |

The other pooling function in our model is maximum pooling, and the pseudocode of the maximum pooling is defined in Algorithm 2.

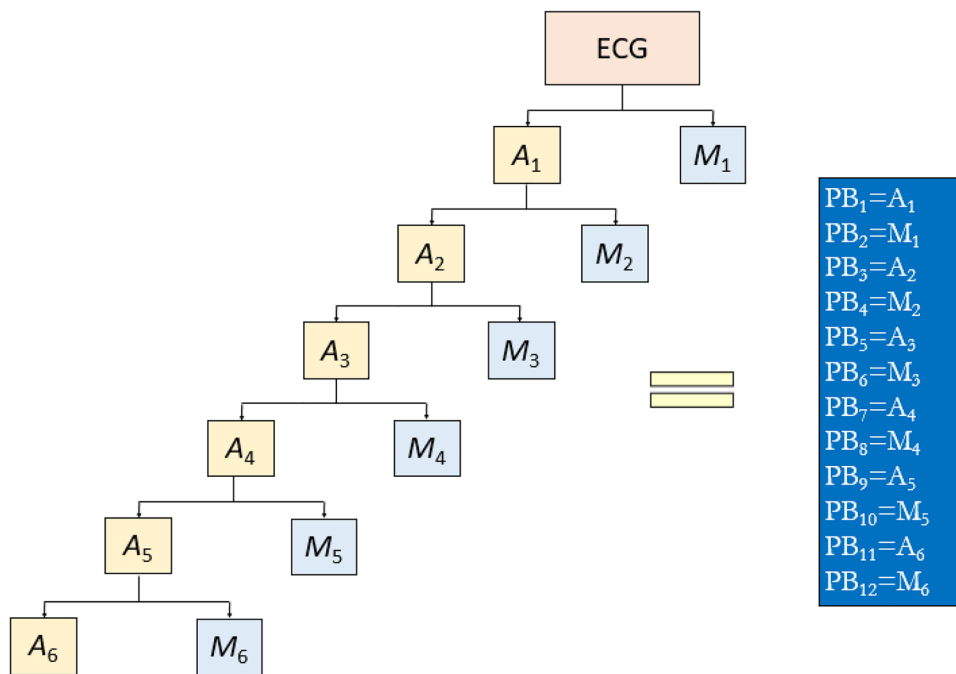
Algorithm 2. Pseudocode of the used maximum pooling.

A pooling band (PB) data structure is created using the decomposed signals generated, as given below.

$$PB_{2h-1} = A_h, \quad (5)$$

|   |
|---|
| <b>Function:</b> $MP(sig)$  |
| <b>Input:</b> One-dimensional signal ( $sig$ ) with a length of $L$ .   |
| <b>Output:</b> The created pooled signal ( $M$ ) with a length of $\lfloor \frac{L}{2} \rfloor$ .   |
| <pre> 00: Load one-dimensional signal. 01: c=1; // Counter defining. 02: for j=1 to L step by 2 do 03:   for t=1 to 2 do 04:     block(t) = sig(t + j - 1); // Non-overlapping block creation. 05:   end for t 06:   M(c) = max(block); 07:   c = c + 1; 08: end for j </pre> |

**Fig. 3** Schema of the MUPTT. By using all A and M subbands, a pooling band structure has been created to extract features



$$PB_{2h} = M_h. \tag{6}$$

The block diagram of the MUPTT with six levels is shown in Fig. 3.

**Step 2:** Generate handcrafted features by deploying a statistical feature generator and 1D-ISBP function.

$$f_1 = merge(stg(ECG), BP(ECG)), \tag{7}$$

$$f_{k+1} = merge(stg(PB_k), BP(PB_k)), k \in \{1, 2, \dots, 12\}, \tag{8}$$

where  $merge(\cdot)$ ,  $stg(\cdot)$ , and  $BP(\cdot)$  represent the feature merging function, statistical feature generation function, and 1D-ISBP feature extraction function, respectively. By using the feature extraction functions ( $stg(\cdot)$  and  $BP(\cdot)$ ), 13 feature vectors ( $f$ ) are generated, each of length 72 ( $=40 + 32$ ). The details of the feature extraction functions used are explained below.

The first feature generator used is the statistical extractor ( $stg(\cdot)$ ). In this function, 20 features are extracted from the signal [23–28]. Thus,  $stg(\cdot)$  extracts 40 ( $=20 \times 2$ ) features. These features are: fuzzy, permutation, Shannon, Kolmogorov–Sinai, Renyi, Tsallis, wavelet and log entropies. Nonlinear features, namely largest Lyapunov exponent and fractal dimension. The linear features namely: average, median, maximum, minimum, variance, skewness, kurtosis, standard deviation, range and energy.

1D-ISBP, the second feature extractor, is used to generate textural features. 1D-ISBP is the improved one-dimensional version of the CSLBP. CSLBP is a good textural feature extraction function. It uses symmetric center values to

extract features, and 16 ( $=2^4$ ) features have been generated by deploying CSLBP. To improve feature extraction ability, we used center symmetric and linear symmetric values in our proposed 1D-ISBP. In this function, overlapping windows with a size of nine are used that are centered at the fifth value. Two-bit categories are generated by deploying a comparison function, and each bit category contains four bits since 1D-ISBP uses two patterns. The extracted bits are then converted to decimal values to obtain two map signals, the histogram of which constitutes the feature vector. Using 1D-ISBP, 32 features are extracted from each signal. The schematic illustration of the 1D-ISBP feature extraction function is shown in Fig. 4.

The steps of this model are;

- 1: Create overlapping windows with a length of nine.
- 2: Extract bits using the defined two patterns (see Fig. 4) and signum function.

$$bit_1(j) = signum(w(j), w(5 + j)), j \in \{1, 2, 3, 4\}, \tag{9}$$

$$bit_2(j) = signum(w(j), w(10 - j)), \tag{10}$$

$$signum(x, y) = \begin{cases} 0, & x - y < 0 \\ 1, & x - y \geq 0 \end{cases} \tag{11}$$

where  $bit_1$  and  $bit_2$  are two bit categories generated and each bit category contains four bits. Equation (9) defines the first pattern, and Eq. (10) defines the second pattern.

3: Calculate two map signals using the created two-bit groups.

$$\text{map}_g(i) = \sum_{j=1}^4 \text{bit}_g(j) \times 2^{j-1}, g \in \{1, 2\}. \tag{12}$$

4: Extract histograms of the generated two maps ( $\text{map}_1, \text{map}_2$ ).

$$h^g = \vartheta(\text{map}^g), g \in \{1, 2\}. \tag{13}$$

Herein  $h^g$  is the histogram of the  $g^{\text{th}}$  map signal with a length of 16,  $\vartheta(\cdot)$  is the histogram extraction function.

5: Merge the generated two histograms to obtain the feature vector.

$$f(j + 16 \times (g - 1)) = h^g(j), j \in \{1, 2, \dots, 16\}, \tag{14}$$

where  $f_v$  defines the textural features generated with a length of 32.

The five steps above define the proposed 1D-ISBP feature extraction function ( $BP(\cdot)$ ).

**Step 3:** Concatenate the extracted feature vectors ( $f$ ) to create the final feature vector ( $\hat{f}$ ).

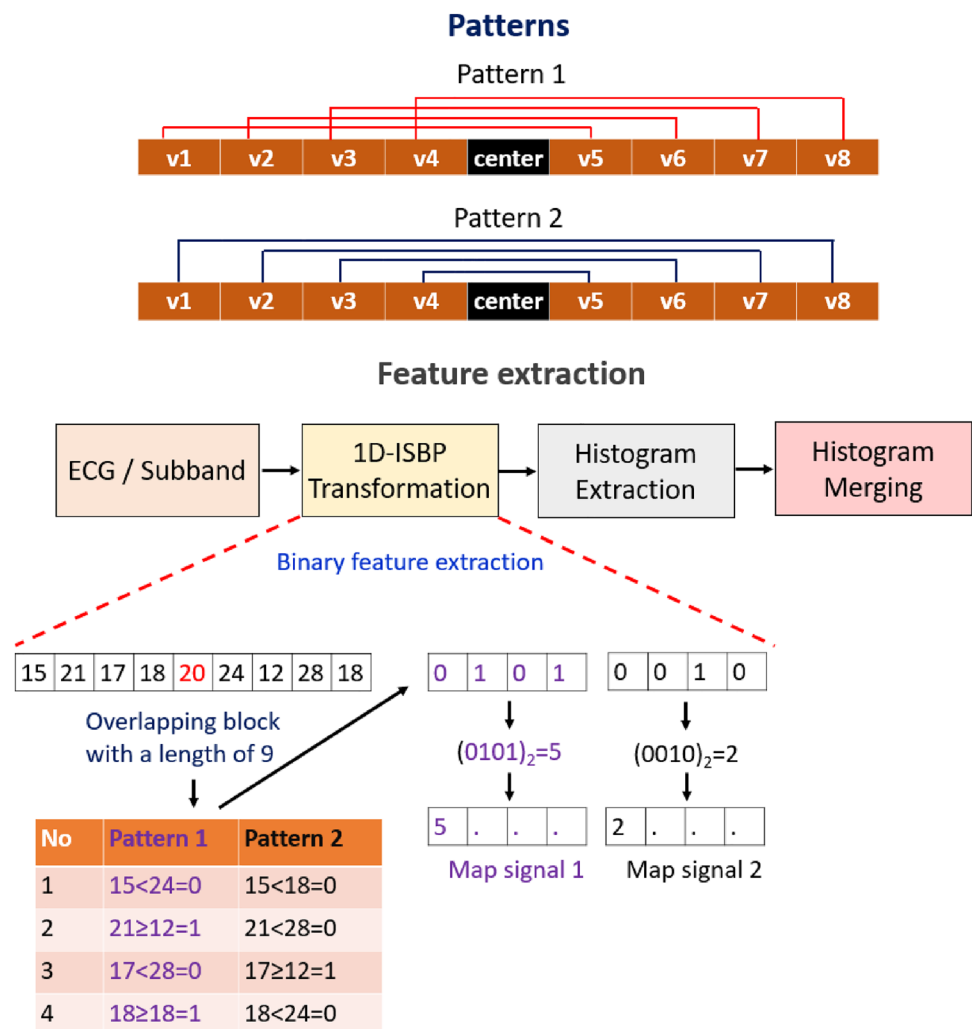
$$\hat{f}_i(j + 72 \times (i - 1)) = f_i(j), j \in \{1, 2, \dots, 72\}, i \in \{1, 2, \dots, 13\}. \tag{15}$$

The steps above define the proposed HHF-MUPTT, which extracts 936 ( $= 72 \times 13$ ) features per beat signal in a single ECG lead.

### 3.2 Feature selection

The primary purpose of this phase is to reduce the number of features without compromising downstream classification performance. For this purpose, we use the feature selection function INCA [29], which is designed to choose the most discriminative feature vectors based on minimal loss/error value calculations. As described by Tuncer et al. [29], INCA improves the feature selection ability of the standard NCA selector [24] by adding a loss function and a loop. In the current study, a feature range is used to decrease the time complexity of the INCA selector. Herein, the range is chosen from 1 to 100. Therefore, 100 feature vectors are selected using INCA, in which a 1NN classifier with ten-fold CV is deployed as the loss/error value calculator.

**Fig. 4** Schema of the feature extraction process using 1D-ISBP. Here,  $v$  defines the values of the overlapping blocks to extract features, and the center defines the center value of the overlapping block



**Step 4:** Choose the best feature vector for each lead using INCA.

### 3.3 Classification

The selected best feature vectors of each lead are classified using a simple distance-based kNN classifier [30], 1NN (hyperparameters:  $k$  is one; distance is L1-norm; voting is equal). In this study, 1NN is utilized both as a classifier and as a loss/error value generator of the INCA selector (see Sect. 3.2).

**Step 5:** Compute lead-wise results by deploying 1NN with a tenfold CV.

### 3.4 Iterative majority voting

IMV algorithm is used to determine the general classification ability of the model [31]. Lead-wise result outputs in Step 5 for all 12 leads that correspond to the same single beat on the source 12-lead ECG are collated and input to the IMV algorithm, which uses a greedy technique to choose the best one that represents the general majority voting. The IMV algorithm used is given in Algorithm 3.

Algorithm 3. IMV algorithm.

|   |
|---|
| <p>Input: Lead-wise results/predicted vectors (<math>r</math>), accuracies of each lead (<math>acc</math>).</p> <p>Output: Voted results (<math>vr</math>).</p>   |
| <pre> 01: Compute qualified indexes (<math>ind</math>) of the results by sorting these vectors according to the <math>acc</math>. 02: <b>for</b> <math>h=3</math> to 12 <b>do</b> // Iterative voting 03:   <b>for</b> <math>i=1</math> to <math>length(r_1)</math> <b>do</b> 04:     <b>for</b> <math>j=1</math> to <math>h</math> <b>do</b> 05:       <math>array(j) = r_{ind(j)}(i)</math>; 06:     <b>end for</b> <math>j</math> 07:     <math>vr_{h-2}(i) = \varphi(array)</math>; // Herein, <math>\varphi(\cdot)</math> is mode function. 08:   <b>end for</b> <math>i</math> 09: <b>end for</b> <math>h</math> </pre> |

**Step 6:** Calculate 10 voted results ( $vr$ ) deploying Algorithm 1.

**Step 7:** Obtain the accuracy of each voted result using  $vr$  and actual output ( $y$ ).

**Step 8:** Choose the best accurate voted result as the general classification result.

The eight steps above define our proposed HHF-based ECG beat classification model for MI classification.

## 4 Performance evaluation

The proposed HHF-MUPTT-based signal classification model is defined in Sect. 3 using eight steps. The experimental setup, performance metrics used lead-wise results, and voted results using IMV are presented in this section.

### 4.1 Experimental setup

The HHF-based ECG classification model was implemented in MATLAB(2021b) environment on a desktop computer with an intel i9 9900 processor, 48 GB memory, 1 TB hard disk, and Windows 10.1 professional operating system without the use of any graphics card or parallel processing technique. We used the following programming functions: MAIN, BP, STG, INCA, KNN, and IMV. By executing the MAIN function, the results were obtained.

### 4.2 Validation

The study dataset comprised 12-lead ECGs that experts had labeled based on manual interpretation of signals from all 12 leads. For classification in this study, these labels were

**Table 3** Lead-wise results (%) and the number of features

| Lead           | Number of features | Accuracy     | UAR          | AP           | Overall F1   | Geometric mean |
|----------------|--------------------|--------------|--------------|--------------|--------------|----------------|
| I              | 96                 | 99.43        | 99.22        | 99.44        | 99.33        | 99.21          |
| II             | 96                 | 97.93        | 97.81        | 97.60        | 97.71        | 97.79          |
| III            | 88                 | <b>99.85</b> | 99.81        | 99.80        | 99.80        | 99.81          |
| aVR            | 84                 | 99.77        | 99.74        | 99.73        | 99.74        | 99.74          |
| aVL            | 95                 | 99.82        | 99.78        | 99.45        | 99.61        | 99.78          |
| aVF            | 88                 | 99.52        | 99.59        | 99.46        | 99.52        | 99.59          |
| V <sub>1</sub> | 95                 | 99.59        | 99.63        | 99.39        | 99.51        | 99.63          |
| V <sub>2</sub> | 87                 | 99.29        | 98.99        | 99.14        | 99.06        | 98.99          |
| V <sub>3</sub> | 85                 | 99.51        | 99.43        | 99.56        | 99.49        | 99.42          |
| V <sub>4</sub> | 78                 | 99.50        | 99.42        | 99.24        | 99.33        | 99.41          |
| V <sub>5</sub> | 100                | 98.75        | 98.46        | 98.35        | 98.40        | 98.44          |
| V <sub>6</sub> | 39                 | 99.83        | <b>99.82</b> | <b>99.84</b> | <b>99.83</b> | <b>99.82</b>   |
| Overall        | 85.91 ± 16.08      | 99.40 ± 0.55 | 99.31 ± 0.62 | 99.25 ± 0.65 | 99.28 ± 0.63 | 99.30 ± 0.62   |

The best results are shown in bold font

UAR unweighted average recall, AP average precision

**Fig. 5** Confusion matrix of Lead III classification results. The enumerated classes are: healthy (0), anterior (1), anterior lateral (2), anterior septal (3), inferior (4), inferior lateral (5), inferior posterior (6), inferior posterior lateral (7), lateral (8), posterior (9) and posterior lateral (10). In addition, the numbers of ECG beats in every myocardial infarct class are given in Table 2

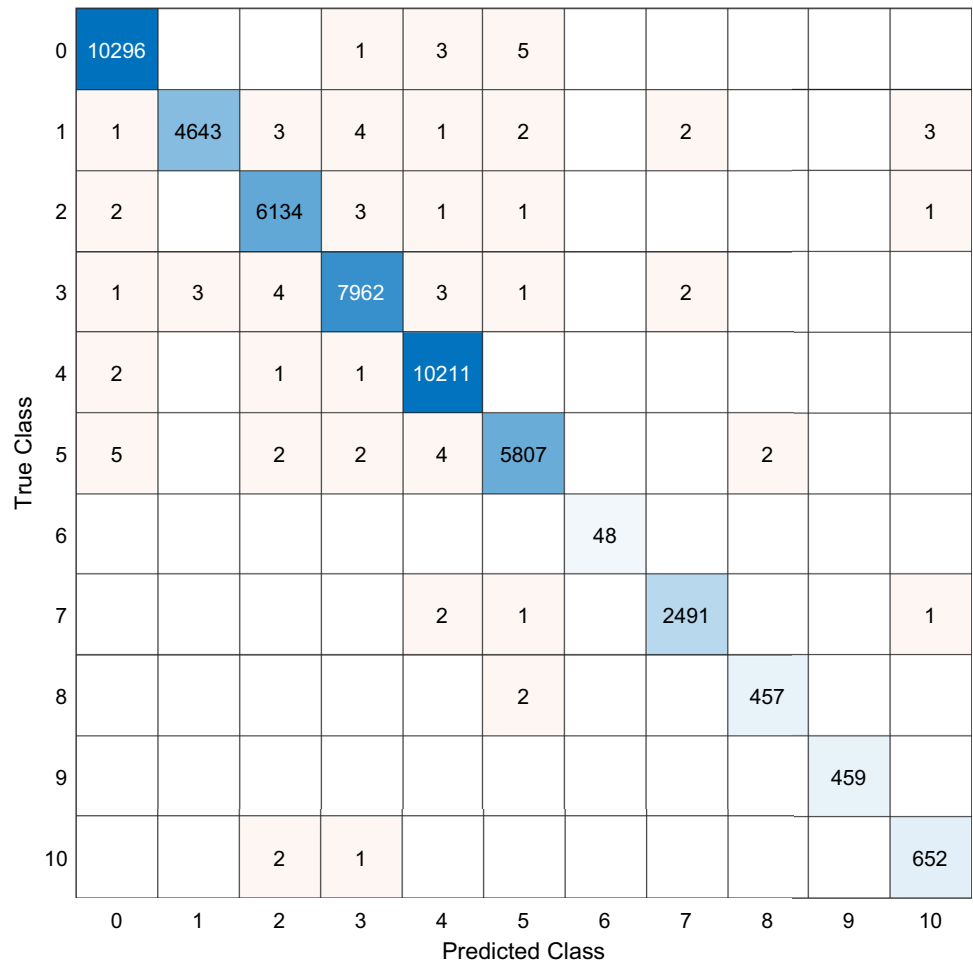


**Fig. 6** Lead-wise classification accuracies using 75:25 split ratio

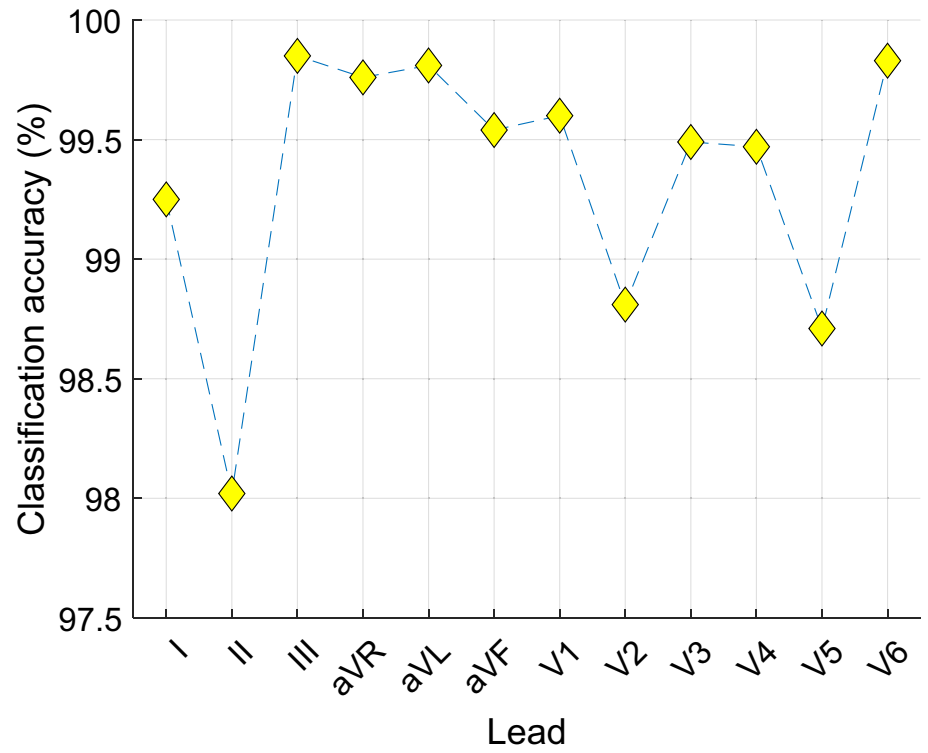


**Fig. 7** Accuracy rates of the calculated ten voted results

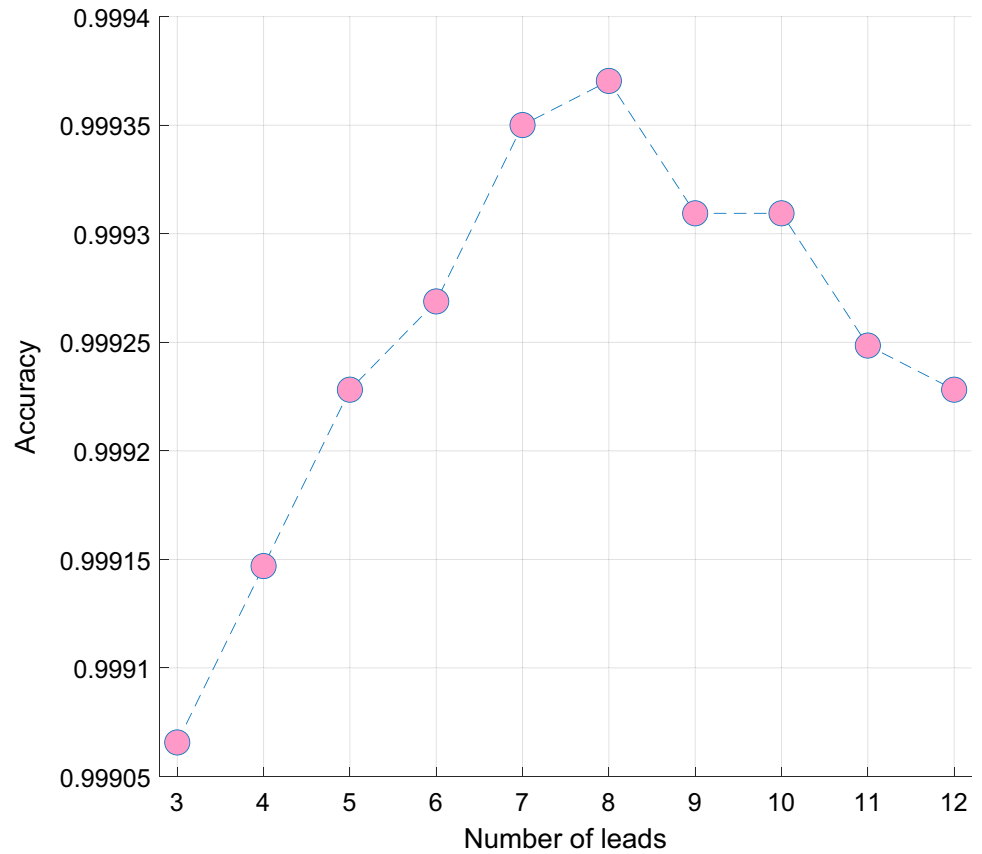


**Fig. 8** Confusion matrix of the best voted result

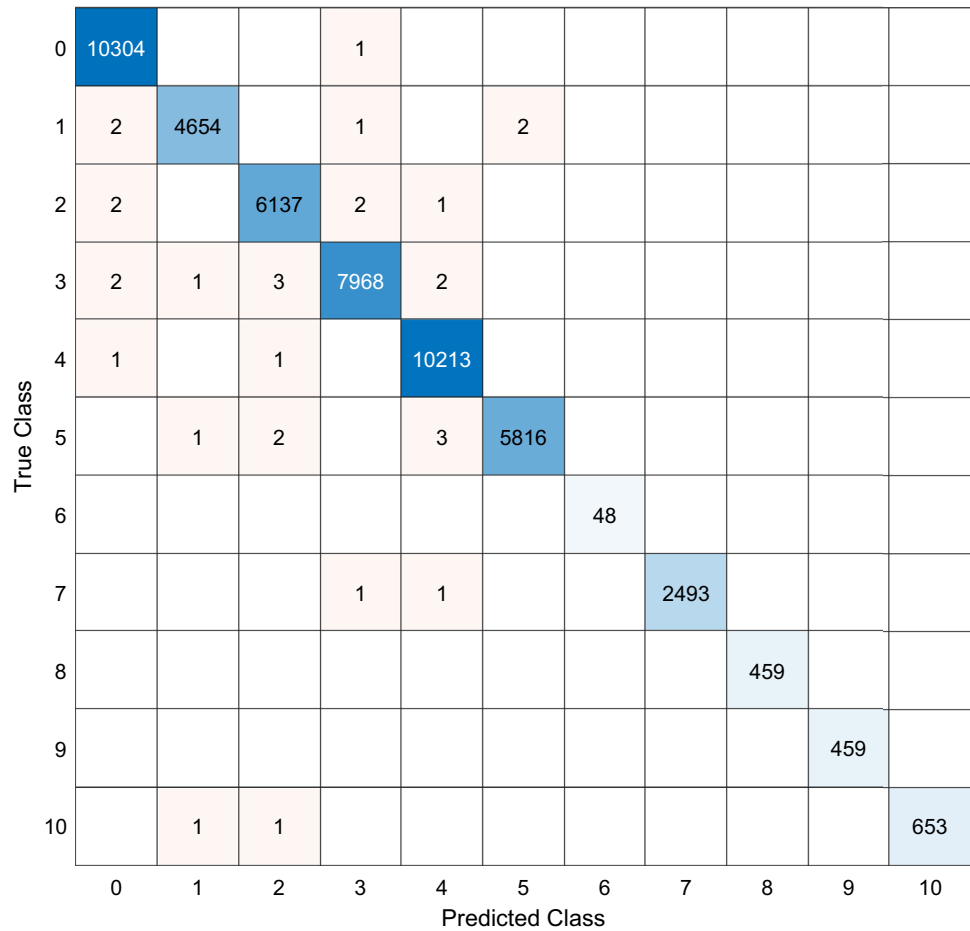


**Table 4** Computational complexity of the proposed HHF-MUPTT-based ECG classification architecture

| Layer              | Computation complexity   |
|--------------------|--------------------------|
| Feature extraction | $O(nd \log nd)$          |
| Feature selection  | $O(kd)$                  |
| Classification     | $O(nd)$                  |
| IMV                | $O(m)$                   |
| Total:             | $O(nd \log nd + kd + m)$ |

In Table 4,  $n$  is the length of the signal,  $d$  defines the number of ECG signals,  $k$  represents the time complexity multiplier of the NCA, and  $m$  is the number of validation prediction vectors

also applied to individual leads of the ECGs. Lead-wise beat classification according to the class labels of individual ECG leads was performed using 1NN with a ten-fold CV. For MI classification based on input from all 12 leads, the best representation from among all 12 lead-wise results corresponding to the same single beat was selected for classification using IMV, with validation being performed using a tenfold CV.

**4.3 Performance metrics**

Standard performance metrics were used to evaluate model performance: accuracy, average recall (UAR), average precision (AP), overall F1 score, and geometric mean [32]. Accuracy is the most popular performance metric. To compare results, we used overall accuracy. As the study dataset is unbalanced, classification accuracy is not adequate for evaluating the performance of the classification model. Therefore, UAR was used. In biomedical datasets, precision is a very important metric for demonstrating the detection rate of disorders, as it represents the ratio of predicted true positives to all positives. Overall F1 score was calculated as the harmonic mean of UAR and AP. One of the important performance evaluation metrics for unbalanced datasets is the geometric mean. It is the geometric mean of the recall (class-wise accuracies) values. Thus, we used the geometric mean to show the performance of our proposal.

**4.4 Lead-wise results**

Optimal feature vectors selected by INCA, which contained a variable number of features (all  $\leq 100$  by design)

depending on the lead, were fed to INN for lead-wise beat classification using tenfold CV. The computed lead-wise results showed fair to excellent performance for MI classification (Table 3), despite the classification being based on single-lead ECG signal inputs. The most discriminative ECG leads were Leads III and V6. The confusion matrix of Lead III classification results (Fig. 5) shows very low misclassification rates.

To show high classification performance of our proposal, we used hold-out validation. Herein, split ratio is selected as 75:25 (75% of the used data have been used for training and 25% out of them have been used for testing). The calculated classification accuracies using hold-out validation have been demonstrated in Fig. 6.

Figure 6 demonstrates that the best lead is III like tenfold CV and our proposal is 99.85% using Lead III. The worst accurate lead per Fig. 6 is Lead II and 98.02% classification accuracy was reached using Lead II. Generally, hold-out validation results are better than tenfold CV results.

#### 4.5 Voted results

For the classification of 12 lead-wise results corresponding to the same single beat, IMV was deployed. Ten voted results were calculated, and the classification accuracies of these results are depicted in Fig. 7. Accuracy rates were at least 99.91% accuracy across all individual voted results. By considering the top 8 leads together and the best representative lead within the group, all performance metrics

(accuracy, geometric mean, average recall, average precision, overall F1-score, and geometric mean) were calculated as 99.94% (accuracy), 99.93% (UAR), 99.96% (AP), 99.94% (overall F1) and 99.93% (geometric mean) respectively. Furthermore, the confusion matrix of the calculated best-voted result is shown in Fig. 8.

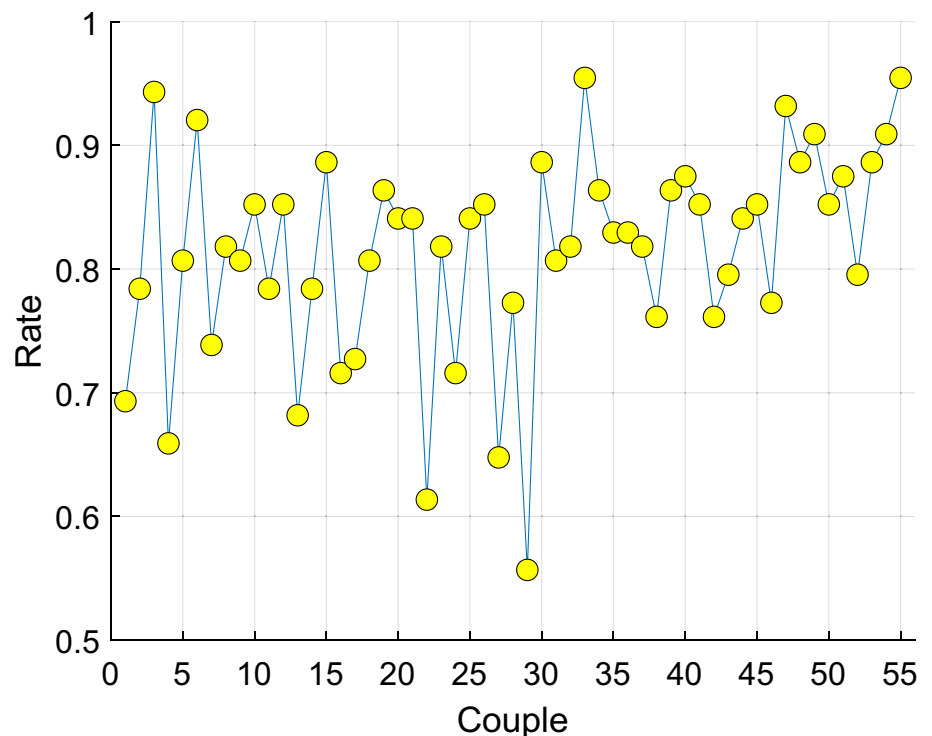
#### 4.6 Time complexity analysis

The last evaluation metric is time complexity analysis, and we used big O notation to measure the computational complexity of our proposed HHF-MUPTT ECG classification model. We mimicked deep learning models to propose the HHF-MUPTT model, but lightweight methods have been used in the proposed architecture. Thus, the time complexity of the HHF-MUPTT ECG classification model is linear. This architecture has four layers, and the time burden was calculated layer by layer in Table 4.

### 5 Discussion

MI causes the death of heart muscle in different parts of the heart depending on the location and distribution of the culprit occluded coronary vessel. In an emergency, the presence and location of MI are diagnosed using widely accessible 12-lead ECGs. MI localization offers clues about the site of the occluded coronary artery and the extent of myocardial involvement, which may inform the choice of approach

**Fig. 9** The informative feature rates for all couples by calculating the t-test



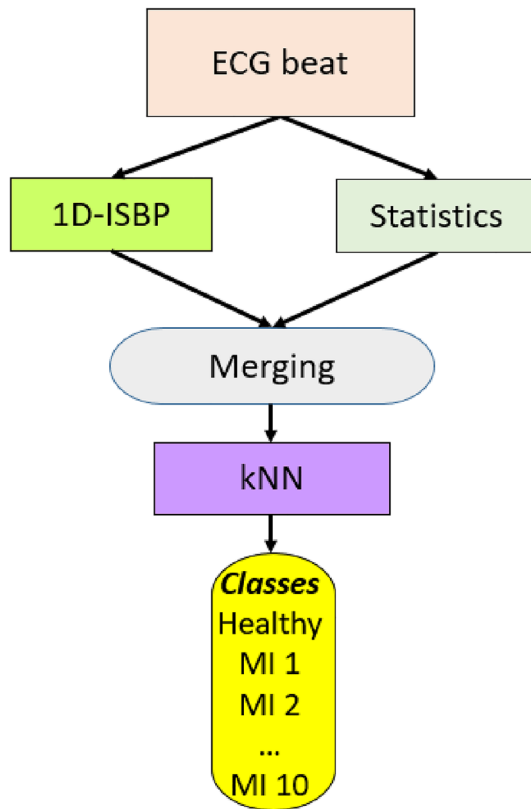


Fig. 10 Overview of the presented alternative model.

during the acute percutaneous coronary intervention and be of prognostic significance, respectively.

The interpretation of ECG for MI diagnosis requires manual interpretation by experts. The latter may not be readily available in rural medical centers or in ambulances. According to guidelines, emergency percutaneous coronary intervention should be performed within 120 min in ST-elevation MI, as any delay significantly increases the risk of mortality and morbidity in MI patients. This leaves very little room for time delay due to difficulty in ECG interpretation. Automated ML-based computer-aided diagnostic tools can facilitate the diagnosis of MI in the emergency setting and are especially helpful for remote applications. With this consideration in mind, ML models that are computationally lightweight may offer the distinct advantage of easier implementation for real-time applications.

This work proposed a new handcrafted ECG beat classification model that attained high classification performance with a low time burden. The proposed HHF-based model uses shallow learning methods and straightforward feature engineering with low time costs. The primary feature extraction functions and MUPTT have time complexities of  $O(n)$  and  $O(n \log n)$ , respectively, using big O notation. These were combined with the INCA feature selector function and 1NN classifier to create the HHF-MUPTT-based model,

which attained at least 97% MI classification accuracy rates on lead-wise beat classification for all 12 ECG leads. Furthermore, our model achieved 99.94% classification accuracy and geometric mean using the IMV algorithm, which analyzed all 12 ECG lead signal inputs associated with the same single beat to output the most representative lead for classification.

### 5.1 Statistical tests for the generated features

To show discriminative attributes of the generated features, a Student t test was performed by calculating the p values. The feature is informative if the p value rate is lower than 0.05. Our dataset used has 11 classes. Therefore, there are  $5.5 \left( = \binom{11}{2} \right)$  couples to show the relationship of the classes. In this test, Lead III was used as it obtained the best performing lead and our model generated 88 features from this lead. Rate of features with a p-value smaller than 0.05 and all features have been calculated for all couples, and the results of this analysis is shown in Fig. 9.

The maximum informative feature rate was calculated as 0.9545 between 3rd (Anterior Septal) and 8th classes (Lateral). All ratios were calculated were higher than 0.5. This analysis demonstrates the high classification abilities of the generated features.

### 5.2 Ablation of our work

In this section, we have presented an alternative model to show the classification performance of our proposal. The alternative model uses 1D-ISBP and statistical feature generation to get classification results. The overview of the alternative model has been demonstrated in Fig. 10 to better understand this model.

This model is applied to Lead III since this is the best performing lead. Our proposed model attained 99.85% classification accuracy using Lead III, but the alternative model (see Fig. 9) reached 81.35% classification accuracy. These results demonstrate that our proposed model reached 18.50% better classification accuracy than this alternative method.

### 5.3 Comparative results

The study dataset was based on the commonly used PhysioBank database [21]. We performed a non-systematic literature review of studies that have used this dataset for ECG beat analysis and compared their performance with our model. Our proposed HHF-MUPTT-based model attained the best classification result among these state-of-the-art models. (Table 5).

**Table 5** Comparison of our developed model with other state-of-the-art methods using the same database

| Study                           | Method   | Validation  | Accuracy (%) |
|---------------------------------|--|-------------|--------------|
| Han and Shi [33]                | Maximal overlap discrete wavelet packet transform  | Tenfold CV  | 99.81        |
| Sridhar et al. [34]             | Pan-Tompkins algorithm, nonlinear features   | Tenfold CV  | 97.96        |
| Halder et al. [35]              | Rule-based rough set method  | Fivefold CV | 99.80        |
| Zhang et al. [36]               | Gramian angular field, principal component analysis network  | Fivefold CV | 99.49        |
| Sharma and Sunkaria [37]        | Stationary wavelet transform, entropy  | Tenfold CV  | 99.76        |
| Zhang et al. [38]               | Stacked sparse autoencoder, bagged tree  | Tenfold CV  | 99.90        |
| Adam et al. [39]                | Relative wavelet nonlinear features  | Tenfold CV  | 99.27        |
| Prabhakararao and Dandapat [40] | Attentional recurrent neural network   |             | 97.79        |
| Sridhar et al. [41]             | Probabilistic neural network   | Tenfold CV  | 98.67        |
| Acharya et al. [42]             | Discrete wavelet transform + entropies + feature selection   | Tenfold CV  | 98.80        |
| Heo et al. [43]                 | Pan-Tompkins algorithm   | Fivefold CV | 96.37        |
| Acharya et al. [44]             | Deep convolutional neural network  | Tenfold CV  | 95.22        |
| Baloglu et al. [45]             | Convolutional neural network   | 70:15:15    | 99.78        |
| Zhang et al. [46]               | Multi-dimensional association information analysis algorithm   | Tenfold CV  | 99.40        |
| Wang et al. [47]                | Statistical feature calculation, entropy, principal component analysis                                     | Tenfold CV  | 99.71        |
| Acharya et al. [48]             | Discrete wavelet transform, empirical mode decomposition, discrete cosine transform                        | Tenfold CV  | 98.50        |
| Kumar et al. [49]               | Flexible analytic wavelet transform framework  | Tenfold CV  | 99.31        |
| Acharya et al. [50]             | Continuous wavelet transform   | Tenfold CV  | 99.55        |
| Rai and Chatterjee [51]         | Convolutional neural network, long short-term memory network   | 80:20       | 99.89        |
| Xiong et al. [52]               | Densely connected convolutional network  | Tenfold CV  | 99.87        |
| Savostin et al. [53]            | Entropy, statistical, probabilistic, and spectral characteristics  | Tenfold CV  | 97.03        |
| Sadhukhan et al. [54]           | Discrete Fourier transforms  | Fivefold CV | 95.60        |
| Lih et al. [55]                 | Convolutional neural network, long short-term memory   | Tenfold CV  | 98.51        |
| Fu et al. [56]                  | Multi-lead attention mechanism, convolutional neural network, bidirectional gated recurrent unit framework | Fivefold CV | 99.93        |
| Sugimoto et al. [57]            | Convolutional auto encoder   | Tenfold CV  | 99.87        |
| Swain et al. [58]               | Stockwell transform, phase distribution pattern  | Unspecified | 99.93        |
| Cao et al. [59]                 | Multichannel lightweight network model   | Tenfold CV  | 96.65        |
| Liu et al. [60]                 | Multiple-feature-branch convolutional bidirectional recurrent neural network                               | Fivefold CV | 93.08        |
| He et al. [61]                  | Convolutional neural networks, active learning   | Fivefold CV | 99.63        |
| Li et al. [62]                  | Convolutional neural networks, generative adversarial networks   | Fivefold CV | 99.06        |
| Liu et al. [63]                 | Evolving multi-branch networks   | Fivefold CV | 97.11        |
| Our method                      | HHF-MUPTT-based ECG classification   | Tenfold CV  | 99.94        |

As can be seen from Table 5, works [40, 44, 45, 51, 52, 55–57, 60, 61] and [62] were used deep learning to achieve high classification ability on the used dataset. Using deep learning techniques Fu et al. [56] attained 99.93% classification accuracy using the attention mechanism. Moreover, the time complexity of their model is exponential. We have proposed a lightweight model, and the time complexity of our model is linear, and we attained 99.94% classification accuracy using this model. Our HHF-MUPTT-based ECG classification model attained the best result for this dataset (see Table 5). To attain high classification performance measurements on this dataset, deep networks were applied

to this dataset. We attained satisfactory classification performance by only using a lightweight model. Furthermore, we attained 99.94% classification accuracy by using fewer features (the number of features for each channel is smaller than 100).

## 5.4 Findings

The salient points of our research are:

- Two new methods have been proposed in this research: MUPTT and 1D-ISBP.

- CSLBP feature creation function uses only symmetric center values to generate 16 features from a signal. In this work, we used center symmetric and linear symmetric values to comprehensively get textural features. Our proposed 1D-ISBP also contains CSLBP features. Therefore, the advantages of the CSLBP features and linear symmetric features have been used in our proposed 1D-ISBP.
- HHF is a multilevel feature extraction method that combines 1D-ISBP, statistical feature generator, and MUPTT to extract distinctive features from ECG beats for MI classification.
- HHF is combined with INCA feature selector and shallow 1NN classification with tenfold CV to output lead-wise classification of MI. In addition, all 12 lead-wise results corresponding to the same ECG beat were fed to IMV algorithm to output the best representative results for MI classification.
- The HHF-MUPTT model is computationally lightweight, rendering it suitable for real-time computer-aided diagnostic applications for remote classification of MI on ECG beat signals in emergency settings.
- Lead-wise results for MI classification using a shallow 1NN classifier. Furthermore, by feeding the lead-wise results of 12 leads associated with the same ECG best to the IMV, the classification accuracy of the HHF-based model was excellent.
- A comprehensive comparison table has been given in Table 4 to highlight the success of the recommended HHF-MUPTT-based ECG classification model.
- The HHF-MUPTT-based model outperforms other state-of-art methods for MI classification using the same dataset. This model also attained better performance than deep models in the literature.

## 6 Conclusions

In this research, a handcrafted MI classification method has been presented, which attained superior classification results that outperformed prior methods trained on the same dataset with 11 classes (one healthy and 10 MI categories). Two new methods have been presented in this research: MUPTT decomposition and 1D-ISBP feature extraction. The HHF-MUPTT-based MI classification model attained excellent lead-wise results overall, with the best lead-wise classification accuracy of 99.85% in Lead III. Moreover, 99.94% accuracy was attained using IMV algorithm. As the model is computationally lightweight, it can potentially be implemented for remote real-time MI diagnosis.

This model is ready for implementation in medical centers since high classification results have been attained. Furthermore, this model has a linear time burden, which makes

it a lightweight ECG signal classification model. By using this model, intelligent ECG devices can be developed that can automatically detect MI and type of MI, potentially saving lives.

**Funding** The authors state that this work has not received any funding.

## Declarations

**Conflict of interest** The authors of this manuscript declare no conflicts of interest.

## References

1. Ribeiro DRP, Cambruzzi E, Schmidt MM, Quadros AS (2016) Thrombosis in ST-elevation myocardial infarction: Insights from thrombi retrieved by aspiration thrombectomy. *World J Cardiol* 8:362
2. Visan I (2018) Myocardial infarct inflammation. *Nat Immunol* 19:99–99
3. Ueda Y, Kosugi S, Abe H, Ozaki T, Mishima T, Date M, Uematsu M, Koretsune Y (2021) Transient increase in blood thrombogenicity may be a critical mechanism for the occurrence of acute myocardial infarction. *J Cardiol* 77:224–230
4. Bentzon JF, Otsuka F, Virmani R, Falk E (2014) Mechanisms of plaque formation and rupture. *Circ Res* 114:1852–1866
5. Rafeian-Kopaei M, Setorki M, Doudi M, Baradaran A, Nasri H (2014) Atherosclerosis: process, indicators, risk factors and new hopes. *Int J Prev Med* 5:927
6. Cuculich PS, Zhang J, Wang Y, Desouza KA, Vijayakumar R, Woodard PK, Rudy Y (2011) The electrophysiological cardiac ventricular substrate in patients after myocardial infarction: non-invasive characterization with electrocardiographic imaging. *J Am Coll Cardiol* 58:1893–1902
7. Sandoval Y, Thygesen K, Jaffe AS (2020) The universal definition of myocardial infarction: present and future. *Circulation* 141:1434–1436
8. Steg P, Juliard J (2005) Primary percutaneous coronary intervention in acute myocardial infarction: time, time, and time! *Heart* 91:993
9. Kobat MA, Karaca O, Barua PD, Dogan S (2021) PrismatoidNet54: an accurate ECG signal classification model using prismatoid pattern-based learning architecture. *Symmetry* 13:1914
10. Baygin M, Tuncer T, Dogan S, Tan R-S, Acharya UR (2021) Automated arrhythmia detection with homeomorphically irreducible tree technique using more than 10,000 individual subject ECG records. *Inf Sci* 575:323–337
11. Subasi A, Dogan S, Tuncer T (2021) A novel automated tower graph based ECG signal classification method with hexadecimal local adaptive binary pattern and deep learning. *J Ambient Intell Humanized Comput* 1–15. <https://doi.org/10.1007/s12652-021-03324-4>
12. Donisi L, Ricciardi C, Cesarelli G, Coccia A, Amitrano F, Adamo S, D'Addio G (2022) Bidimensional and tridimensional Poincaré maps in cardiology: a multiclass machine learning study. *Electronics* 11:448
13. Huang D, Zheng S, Liu Z, Zhu K, Zhi H, Ma G (2022) Machine learning revealed ferroptosis features and a novel ferroptosis-based classification for diagnosis in acute myocardial infarction. *Front Genet* 13:813438–813438

14. Swetha A, Santhi B, Brindha G (2022) Machine learning and deep learning for medical analysis—a case study on heart disease data, fundamentals and methods of machine and deep learning: algorithms, tools and applications 177–209. <https://doi.org/10.1002/9781119821908.ch8>
15. Rahman T, Akinbi A, Chowdhury ME, Rashid TA, Şengür A, Khandakar A, Islam KR, Ismael AM (2022) COV-ECGNET: COVID-19 detection using ECG trace images with deep convolutional neural network. *Health Inform Sci Syst* 10:1–16
16. Jahmunah V, Ng E, San TR, Acharya UR (2021) Automated detection of coronary artery disease, myocardial infarction and congestive heart failure using GaborCNN model with ECG signals. *Comput Biol Med* 134:104457
17. Gibson CM, Mehta S, Ceschim MR, Frauenfelder A, Vieira D, Botelho R, Fernandez F, Villagran C, Niklitschek S, Matheus CI (2022) Evolution of single-lead ECG for STEMI detection using a deep learning approach. *Int J Cardiol* 346:47–52
18. Sharma M, San Tan R, Acharya UR (2018) A novel automated diagnostic system for classification of myocardial infarction ECG signals using an optimal biorthogonal filter bank. *Compute Biol Med* 102:341–356
19. Darmawahyuni A, Nurmaini S (2019) Deep learning with long short-term memory for enhancement myocardial infarction classification, 2019 6th International Conference on Instrumentation, Control, and Automation (ICA), IEEE, pp. 19–23.
20. Heikkilä M, Pietikäinen M, Schmid C (2009) Description of interest regions with local binary patterns. *Pattern Recogn* 42:425–436
21. Goldberger AL, Amaral LA, Glass L, Hausdorff JM, Ivanov PC, Mark RG, Mietus JE, Moody GB, Peng C-K, Stanley HE (2000) PhysioBank, PhysioToolkit, and PhysioNet: components of a new research resource for complex physiologic signals. *Circulation* 101:e215–e220
22. Pan J, Tompkins W (1985) A real-time QRS detection algorithm. *IEEE Transact Biomed Eng* 32:230
23. Kuncan F, Yılmaz K, Kuncan M (2019) New approaches based on local binary patterns for gender identification from sensor signals. *J Faculty Eng Archit Gazi Univ* 34:2173–2186
24. Zhang Z, Yeung RW (1998) On characterization of entropy function via information inequalities. *IEEE Trans Inf Theory* 44:1440–1452
25. Rockinger M, Jondeau E (2002) Entropy densities with an application to autoregressive conditional skewness and kurtosis. *J Economet* 106:119–142
26. Usta I, Kantar YM (2011) Mean-variance-skewness-entropy measures: a multi-objective approach for portfolio selection. *Entropy* 13:117–133
27. Taşçı B, Acharya MR, Barua PD, Yildiz AM, Gun MV, Keles T, Dogan S, Tuncer T (2022) A new lateral geniculate nucleus pattern-based environmental sound classification using a new large sound dataset. *Appl Acoust* 196:108897
28. Aydemir E, Tuncer T, Dogan S, Gururajan R, Acharya UR (2021) Automated major depressive disorder detection using melamine pattern with EEG signals. *Appl Intell* 51:6449–6466
29. Tuncer T, Dogan S, Özyurt F, Belhaouari SB, Bensmail H (2020) Novel multi center and threshold ternary pattern based method for disease detection method using voice. *IEEE Access* 8:84532–84540
30. Peterson LE (2009) K-nearest neighbor. *Scholarpedia* 4:1883
31. Dogan A, Akay M, Barua PD, Baygin M, Dogan S, Tuncer T, Dogru AH, Acharya UR (2021) PrimePatNet87: prime pattern and tunable q-factor wavelet transform techniques for automated accurate EEG emotion recognition. *Comput Biol Med* 138:104867
32. Powers DM (2020) Evaluation: from precision, recall and F-measure to ROC, informedness, markedness and correlation, arXiv preprint [arXiv:2010.16061](https://arxiv.org/abs/2010.16061)
33. Han C, Shi L (2019) Automated interpretable detection of myocardial infarction fusing energy entropy and morphological features. *Comput Methods Programs Biomed* 175:9–23
34. Sridhar C, Lih OS, Jahmunah V, Koh JE, Ciaccio EJ, San TR, Arunkumar N, Kadry S, Rajendra Acharya U (2021) Accurate detection of myocardial infarction using non linear features with ECG signals. *J Ambient Intell Humanized Comput* 12:3227–3244
35. Halder B, Mitra S, Mitra M (2019) Classification of complete myocardial infarction using rule-based rough set method and rough set explorer system. *IETE J Res* 68:1–11
36. Zhang G, Si Y, Wang D, Yang W, Sun Y (2019) Automated detection of myocardial infarction using a gramian angular field and principal component analysis network. *IEEE Access* 7:171570–171583
37. Sharma L, Sunkaria R (2020) Myocardial infarction detection and localization using optimal features based lead specific approach. *Irbm* 41:58–70
38. Zhang J, Lin F, Xiong P, Du H, Zhang H, Liu M, Hou Z, Liu X (2019) Automated detection and localization of myocardial infarction with staked sparse autoencoder and treebagger. *IEEE Access* 7:70634–70642
39. Adam M, Oh SL, Sudarshan VK, Koh JE, Hagiwara Y, Tan JH, San Tan R, Acharya UR (2018) Automated characterization of cardiovascular diseases using relative wavelet nonlinear features extracted from ECG signals. *Comput Methods Programs Biomed* 161:133–143
40. Prabhakararao E, Dandapat S (2020) Myocardial infarction severity stages classification from ecg signals using attentional recurrent neural network. *IEEE Sens J* 20:8711–8720
41. Sridhar C, Acharya UR, Fujita H, Bairy GM (2016) Automated diagnosis of coronary Artery Disease using nonlinear features extracted from ECG signals. 2016 IEEE International Conference on Systems, Man, and Cybernetics (SMC), IEEE, pp. 000545–000549
42. Acharya UR, Fujita H, Sudarshan VK, Oh SL, Adam M, Koh JE, Tan JH, Ghista DN, Martis RJ, Chua CK (2016) Automated detection and localization of myocardial infarction using electrocardiogram: a comparative study of different leads. *Knowl-Based Syst* 99:146–156
43. Heo J, Lee JJ, Kwon S, Kim B, Hwang SO, Yoon YR (2020) A novel method for detecting ST segment elevation myocardial infarction on a 12-lead electrocardiogram with a three-dimensional display. *Biomed Signal Process Control* 56:101700
44. Acharya UR, Fujita H, Oh SL, Hagiwara Y, Tan JH, Adam M (2017) Application of deep convolutional neural network for automated detection of myocardial infarction using ECG signals. *Inf Sci* 415:190–198
45. Baloglu UB, Talo M, Yildirim O, San Tan R, Acharya UR (2019) Classification of myocardial infarction with multi-lead ECG signals and deep CNN. *Pattern Recogn Lett* 122:23–30
46. Zhang J, Liu M, Xiong P, Du H, Zhang H, Lin F, Hou Z, Liu X (2021) A multi-dimensional association information analysis approach to automated detection and localization of myocardial infarction. *Eng Appl Artif Intell* 97:104092
47. Wang Z, Qian L, Han C, Shi L (2020) Application of multi-feature fusion and random forests to the automated detection of myocardial infarction. *Cogn Syst Res* 59:15–26
48. Acharya UR, Fujita H, Adam M, Lih OS, Sudarshan VK, Hong TJ, Koh JE, Hagiwara Y, Chua CK, Poo CK (2017) Automated characterization and classification of coronary artery disease and myocardial infarction by decomposition of ECG signals: a comparative study. *Inf Sci* 377:17–29
49. Kumar M, Pachori RB, Acharya UR (2017) Automated diagnosis of myocardial infarction ECG signals using sample entropy in flexible analytic wavelet transform framework. *Entropy* 19:488

50. Acharya UR, Fujita H, Sudarshan VK, Oh SL, Adam M, Tan JH, Koo JH, Jain A, Lim CM, Chua KC (2017) Automated characterization of coronary artery disease, myocardial infarction, and congestive heart failure using contourlet and shearlet transforms of electrocardiogram signal. *Knowl-Based Syst* 132:156–166
51. Rai HM, Chatterjee K (2021) Hybrid CNN-LSTM deep learning model and ensemble technique for automatic detection of myocardial infarction using big ECG data. *Appl Intell* 52:1–19
52. Xiong P, Xue Y, Zhang J, Liu M, Du H, Zhang H, Hou Z, Wang H, Liu X (2021) Localization of myocardial infarction with multi-lead ECG based on DenseNet. *Comput Methods Programs Biomed* 203:106024
53. Savostin A, Ritter D, Savostina G (2019) Using the k-nearest neighbors algorithm for automated detection of myocardial infarction by electrocardiogram data entries. *Pattern Recognit Image Anal* 29:730–737
54. Sadhukhan D, Pal S, Mitra M (2018) Automated identification of myocardial infarction using harmonic phase distribution pattern of ECG data. *IEEE Trans Instrum Meas* 67:2303–2313
55. Lih OS, Jahmunah V, San TR, Ciaccio EJ, Yamakawa T, Tanabe M, Kobayashi M, Faust O, Acharya UR (2020) Comprehensive electrocardiographic diagnosis based on deep learning. *Artif Intell Med* 103:101789
56. Fu L, Lu B, Nie B, Peng Z, Liu H, Pi X (2020) Hybrid network with attention mechanism for detection and location of myocardial infarction based on 12-lead electrocardiogram signals. *Sensors* 20:1020
57. Sugimoto K, Kon Y, Lee S, Okada Y (2019) Detection and localization of myocardial infarction based on a convolutional autoencoder. *Knowl-Based Syst* 178:123–131
58. Swain SS, Patra D, Singh YO (2020) Automated detection of myocardial infarction in ECG using modified Stockwell transform and phase distribution pattern from time-frequency analysis. *Biocybernetics and Biomedical Engineering* 40:1174–1189
59. Cao Y, Wei T, Zhang B, Lin N, Rodrigues JJ, Li J, Zhang D (2021) ML-Net: multi-channel lightweight network for detecting myocardial infarction. *IEEE J Biomed Health Inform* 25:3721–3731
60. Liu W, Wang F, Huang Q, Chang S, Wang H, He J (2019) MFB-CBRNN: A hybrid network for MI detection using 12-lead ECGs. *IEEE J Biomed Health Inform* 24:503–514
61. van Hespden KM, Zwanenburg JJ, Dankbaar JW, Geerlings MI, Hendrikse J, Kuijf HJ (2021) An anomaly detection approach to identify chronic brain infarcts on MRI. *Sci Rep* 11:1–10
62. Li W, Tang YM, Yu KM, To S (2022) SLC-GAN: an automated myocardial infarction detection model based on generative adversarial networks and convolutional neural networks with single-lead electrocardiogram synthesis. *Inform Sci* 589:738–750
63. Liu W, Ji J, Chang S, Wang H, He J, Huang Q (2022) EvoMBN: evolving multi-branch networks on myocardial infarction diagnosis using 12-lead electrocardiograms. *Biosensors* 12:15

**Publisher's Note** Springer Nature remains neutral with regard to jurisdictional claims in published maps and institutional affiliations.

Springer Nature or its licensor (e.g. a society or other partner) holds exclusive rights to this article under a publishing agreement with the author(s) or other rightsholder(s); author self-archiving of the accepted manuscript version of this article is solely governed by the terms of such publishing agreement and applicable law.

## Authors and Affiliations

Prabal Datta Barua<sup>1,2</sup> · Emrah Aydemir<sup>3</sup> · Sengul Dogan<sup>4</sup>  · Mehmet Ali Kobat<sup>5</sup> · Fahrettin Burak Demir<sup>6</sup> · Mehmet Baygin<sup>7</sup> · Turker Tuncer<sup>4</sup> · Shu Lih Oh<sup>8</sup> · Ru-San Tan<sup>9,10</sup> · U. Rajendra Acharya<sup>8,11,12</sup>

Prabal Datta Barua  
prabal.barua@usq.edu.au

Emrah Aydemir  
emrahaydemir@sakarya.edu.tr

Mehmet Ali Kobat  
mkobat@firat.edu.tr

Fahrettin Burak Demir  
fdemir@bandirma.edu.tr

Mehmet Baygin  
mehmetbaygin@ardahan.edu.tr

Turker Tuncer  
turkertuncer@firat.edu.tr

Shu Lih Oh  
shulih@hotmail.com

Ru-San Tan  
tanrsnhc@gmail.com

U. Rajendra Acharya  
aru@np.edu.sg

<sup>2</sup> Faculty of Engineering and Information Technology, University of Technology Sydney, Sydney, NSW 2007, Australia

<sup>3</sup> Department of Management Information, College of Management, Sakarya University, Sakarya, Turkey

<sup>4</sup> Department of Digital Forensics Engineering, Technology Faculty, Firat University, Elazig, Turkey

<sup>5</sup> Department of Cardiology, Firat University Hospital, Firat University, 23119 Elazig, Turkey

<sup>6</sup> Department of Software Engineering, Faculty of Engineering and Natural Sciences, Bandirma Onyedi Eylul University, Bandirma, Turkey

<sup>7</sup> Department of Computer Engineering, College of Engineering, Ardahan University, Ardahan, Turkey

<sup>8</sup> Department of Electronics and Computer Engineering, Ngee Ann Polytechnic, Singapore 599489, Singapore

<sup>9</sup> Department of Cardiology, National Heart Centre Singapore, Singapore, Singapore

<sup>10</sup> Duke-NUS Medical School, Singapore, Singapore

<sup>11</sup> Department of Biomedical Engineering, School of Science and Technology, SUSS University, Singapore, Singapore

<sup>12</sup> Department of Biomedical Informatics and Medical Engineering, Asia University, Taichung, Taiwan

<sup>1</sup> School of Business (Information System), University of Southern Queensland, Toowoomba, QLD 4350, Australia